BioEnergy Research (2019) 12:370–387
https://doi.org/10.1007/s12155-019-09974-9

Comprehensive Kinetic Study on the Pyrolysis and Combustion Behaviours of Five Oil Palm Biomass by Thermogravimetric-Mass Spectrometry (TG-MS) Analyses

Megan Soh[1] · Jiuan Jing Chew[1] · Shaomin Liu[2] · Jaka Sunarso[1]

Published online: 28 March 2019

Abstract

Thermochemical conversion process is one of the most promising routes to harness the potential of oil palm biomass as renewable energy alternative in Malaysia. Despite this potential, there is a lack of comprehensive study that characterises the complete spectrum of oil palm biomass. In this work, thermogravimetric-mass spectrometry (TG-MS) results of five oil palm biomass, i.e., oil palm trunk (OPT), palm kernel shell (PKS), oil palm frond (OPF), mesocarp fibre (MF) and empty fruit bunch (EFB), in pyrolysis and combustion conditions are presented and analysed. Kinetic studies on the TG data of these biomass were performed using Coats–Redfern integral method and Šesták–Berggren function to determine the activation energy and the reaction mechanism at different thermal decomposition stages. Pyrolysis of hemicellulose, cellulose, and lignin occurs at 140–331, 235–435, and 380–600 °C, respectively, while combustion of hemicellulose, cellulose, and lignin took place at 140–313, 225–395, and 372–600 °C, respectively. The activation energy was the highest for cellulose decomposition in both pyrolysis and combustion cases. Phase boundary reaction dominated during hemicellulose and cellulose decompositions, while nucleation dominated during lignin decomposition and char oxidation. MS results show that majority of the gases came out between 250 and 600 °C, mainly from CH_4 and H_2O in pyrolysis case and from CH_4, CO_2 and H_2O in combustion case. Other than these major gases, NO, NO_2 and SO_2 were also generated although in much lower proportion compared to these gases. Based on TG-MS results, the best potential application for each biomass was also identified where OPT and OPF are suggested for gasification and fermentation, PKS for bio-char production and combustion, MF for bio-oil production, combustion, and bio-char production and EFB for bio-oil and bio-char production.

Keywords Kinetics · Oil palm biomass · Pyrolysis · Combustion · TG-MS

Background

Approximately 4.49 million ha of land is dedicated to oil palm cultivation in Malaysia [1], which accounts for 58% of the total agriculture land in 2012 [2]. This makes the nation the second largest producer and exporter of palm oil [3]. The milling process for the extraction of palm oil generates various oil palm biomass, such as empty fruit bunches (EFB), palm kernel shell (PKS), and mesocarp fibre (MF) [4, 5]. For every tonne of palm oil produced, approximately 1 t of EFB and 0.6 t of MF are created, respectively. Likewise, 0.9 t of PKS is generated per tonne of palm kernel oil produced [6]. Other oil palm biomass, such as oil palm trunks (OPT) and oil palm fronds (OPF), are also produced from the plantation site during harvesting and replantation seasons [4, 5]. Up to 75 t of OPT and OPF are obtained for every hectare of cultivated land from the plantation site [7].

These oil palm biomass can be utilised as a renewable energy alternative to fossil fuel-based resources, such as coal, petroleum and natural gas [8]. Three main conversion processes are available to convert biomass into usable energy—thermochemical, biochemical and physiochemical [9]. Among

Electronic supplementary material The online version of this article (https://doi.org/10.1007/s12155-019-09974-9) contains supplementary material, which is available to authorized users.

✉ Jiuan Jing Chew
jchew@swinburne.edu.my

✉ Jaka Sunarso
jsunarso@swinburne.edu.my

[1] Faculty of Engineering, Computing and Science, Research Centre for Sustainable Technologies, Swinburne University of Technology Sarawak Campus, 93350 Kuching, Sarawak, Malaysia

[2] Department of Chemical Engineering, Curtin University, Perth, WA 6845, Australia

these processes, thermochemical conversion is generally preferred given the possibility to directly utilise the entire biomass feedstock without any chemical pre-treatment, sterilisation and long processing time [10]. Different products for different applications can be obtained depending on the type of thermochemical conversion used, such as pyrolysis, combustion, gasification and liquefaction. Pyrolysis is the thermal degradation of organic materials in the absence of oxygen [10], also known as non-oxidative thermal degradation. The cracking of polymeric structure that occurs during pyrolysis generates three main products, i.e., volatile fraction (i.e., gases and vapour), liquid fraction and char [11]. Pyrolysis has regained its popularity, recently, given its ability to produce liquid fuel that can be stored and transported easily. The pyrolytic liquid (bio-oil) can be further upgraded to produce transportation fuel [12]. Combustion represents another thermochemical conversion process that is performed in the presence of oxygen. Combustion of oil palm biomass is a well-established process that has been used in palm oil mills to reduce fossil fuel dependency for electricity generation and as a solution for solid waste management [13]. The inherent variation in the property and composition of biomass is anticipated to affect the product and performance of pyrolysis and combustion [14]. Reactor design has an important role in maintaining the consistency of the product since different reactor configuration leads to distinct product yield and characteristics [15].

Kinetic modelling can provide insights on the dominant reaction variables and the effect of operating condition, which serve as a guide to optimise the reactor design for a particular biomass [16]. Model fitting method can be used to determine the kinetic parameters and the most plausible reaction mechanism for complex biomass degradation. The reaction mechanism is normally determined by identifying a model function that can describe the thermal decomposition behaviour for complex biomass [17]. A global model expression proposed by Šesták and Berggren [18], for instance, has been used to correlate heterogeneous non-isothermal solid-state reaction [19]. Kinetic modelling of solid biomass often makes use of the thermogravimetric analysis (TGA) technique that reveals their thermal degradation characteristics [20]. Numerous studies on the kinetics of oil palm biomass using TGA are available [11, 16, 21]. Lee et al. [21] have investigated the potential of using PKS, EFB and palm oil sludge as a potential feedstock to produce bio-char through slow pyrolysis using TGA. They utilised the iso-conversional Kissinger–Akahira–Sunose (KAS) and Flynn–Wall–Ozawa (FWO) models to evaluate the pyrolysis kinetics and concluded that activation energy obtained from these models was highly influenced by the degree of conversion. Guo and Lua [16] reported the kinetic studies of PKS pyrolysis using one-step global model and two-step consecutive model, whereas Luangkiattikhun et al. [11] investigated the thermal degradation of PKS, oil palm fibre (OPF) and oil palm kernel (OPK) using two-parallel reaction model, one-step global model and two-step consecutive model. The kinetics of the oil palm biomass thermal degradation in both studies are closely tied to their thermal evolution profiles. In Guo and Lua's [16] case, one-step global model can predict the pyrolysis of PKS only on the low temperature regime while two-step consecutive reaction model performs better across both low- and high-temperature regimes. In Luangkiattikhun et al.'s [11] case, one-step global model was only able to describe the pyrolysis of OPK and two-parallel reactions model was required to describe the pyrolysis of PKS and OPF.

Thermal degradation of oil palm biomass is complex due to the simultaneous occurrence of several reactions [14]. The variation in the thermal behaviour of different biomass reflects the differences in their physical and chemical properties [22]. Identifying the product distribution of the oil palm biomass at a thermal decomposition stage becomes essential to accomplish optimised reactor performance, which cannot be achieved using TGA alone. The use of in situ mass spectrometry (MS) to detect the gas products released during the thermal degradation in thermogravimetric-mass spectrometry (TG-MS) can provide supplementary information to determine the reactions that are captured in TGA data [23]. In such TG-MS studies, the gas evolution profile can be correlated to the thermal behaviour of the main functional groups in the feedstock [23–26] .

To date, only two studies have been performed on the pyrolysis and combustion of oil palm biomass using TG-MS [26, 27]. Asadieraghi and Daud [26] performed TG-MS study on the pyrolysis of three oil palm biomass (i.e., PKS, EFB and MF). They assumed a first-order reaction for their kinetics study and devised the plausible reactions based on the evolution profiles of the three main permanent gases (i.e., CO_2, CO and H_2). Thermal degradation of oil palm biomass was reported to occur in three stages, i.e., moisture removal, slow depolymerisation and complex thermal decomposition. Their MS results revealed that the permanent gases were mainly produced in the third stage from the cleavage of oxygenated functional groups and the secondary reactions. Aghamohammadi et al. [27] used TG-MS to capture the combustion and gas distribution profile of five woody biomass, i.e., OPT, mixed tropical wood residue from sawmill (MTW), bamboo, acacia and rubber wood (RW). They reported that the combustion of these biomass generates CO, CO_2, CH_3CO^+, $COOH^+$, CH_4 and H_2O. H_2O and CO_2 were the main products, although the latter was generated mainly during the devolatilisation stage. They also observed that OPT exhibits H_2O and CH_4 evolution and thermal decomposition profiles that are distinct from the other biomass. Despite their insightful findings, an overall, more integrated study with a postulated mechanism that captures the trends from both TG and MS data from a more representative spectrum of oil palm biomass is required.

In this work, characterisation of five oil palm biomass (i.e., OPT, OPF, EFB, MF and PKS) is performed and correlated to their thermal decomposition behaviour during pyrolysis and combustion by TG analyses. The pyrolysis and combustion kinetic parameters and reaction mechanism of the five oil palm biomass are evaluated by the model fitting method. Furthermore, the gases evolved during thermal decomposition are analysed by MS. Finally, the five oil palm biomass potential application in thermochemical conversion processes is identified based on the TG-MS results obtained in this study.

Experimental Section

Materials and Methods

The five oil palm biomass used in this study are oil palm trunk (OPT), oil palm frond (OPF), empty fruit bunches (EFB), mesocarp fibre (MF) and palm kernel shell (PKS) obtained from palm oil mills and oil palm estate in Sarawak, Malaysia. EFB, MF and PKS were obtained from the Samarahan Felcra Palm Oil Mill (Kilang Sawit Felcra Berhad Samarahan). The OPF was obtained from KPF Palm Oil Mill Sdn. Bhd. located in Samarahan, while OPT was obtained from an oil palm estate in Similajau, Bintulu. The collected samples were oven-dried at 105 °C for 24 h to reduce the moisture content. Subsequently, the dried samples were milled and sieved to the required size range. The milled samples were kept in a sealed bag and kept in a desiccator until further use.

Analysis

Oil Palm Biomass Characterisation

Proximate analysis was performed following the procedure described in ASTM D1762-84. Elemental analysis of the biomass was recorded by a CHNS instrument (Elementar Analysensysteme GmbH, varioMICRO). The oxygen content was estimated as the difference between 100% with the total C, H, N and S contents. The proximate analysis and elemental analysis were performed in triplicate and duplicate, respectively.

Thermogravimetric-Mass Spectrometry (TG-MS)

The thermal decomposition of oil palm biomass samples was carried out in a thermal gravimetric analysis (TGA) apparatus (Mettler Toledo, TGA/SDTA 851^e) coupled to a quadrupole mass spectrometer (Pfeiffer Vacuum, ThermoStar GSD 301 T2) with mass resolution limit of 1 a.m.u. and detection limit less than 20 ppm to analyse the mass changes and evolved decomposition gas with respect to temperature. The TG-MS studies used samples with particle size below 150 μm. The transfer lines between the TGA and MS were heated to 200 °C to avoid the presence of cold spots and to maintain the evolved products in the gaseous phase. The ion source was operated at 70 eV. Nitrogen gas and compressed air were used for pyrolysis and combustion experiments, respectively. Approximately, 10 mg of sample was placed in an aluminium crucible and heated inside the TG furnace from 30 to 1000 °C at a heating rate of 10 °C/min. Residual and derivative weights of the sample with respect to time and temperature were recorded. The mass analysis was performed for mass spectra range up to 200 a.m.u.

Kinetic Analysis

Oil palm biomass have complex structures and tend to exhibit multi-step reactions during thermal degradation, and different activation energies were postulated for the different steps involved. The effective activation energy and the overall reaction rate vary with temperature and extent of reaction [17]. Due to the complexity of oil palm biomass reactions, the kinetic parameters of oil palm biomass degradation under oxidative and non-oxidative atmosphere were obtained in two steps, i.e., estimation of activation energy, followed by determination of kinetic model.

Estimation of Activation Energy

The reaction rate for the thermal decomposition of solid-state materials can be expressed as a function of temperature, T, and the extent of conversion, α, as follows:

$$\frac{d\alpha}{dt} = \mathrm{k(T)}f(\alpha) \tag{1}$$

where t is the instantaneous time of the pyrolysis or combustion process, α is the extent of conversion and $f(\alpha)$ is the function of the reaction model that has various reaction mechanism descriptions. The extent of conversion α can be expressed as:

$$\alpha = \frac{w_0 - w}{w_0 - w_\mathrm{f}} \tag{2}$$

where w_0, w and w_f are the initial, instantaneous and final masses of the oil palm biomass samples, respectively.

The reaction rate constant, k, that is temperature-dependant can be expressed by the following Arrhenius equation:

$$k = A\exp\left(-\frac{E_\mathrm{a}}{RT}\right) \tag{3}$$

where the kinetic parameters A and E_a are the Arrhenius pre-exponential factor and the activation energy, respectively. The constant, R, is the universal gas constant, and T is the

instantaneous (pyrolysis or combustion) temperature. For non-isothermal condition where constant heating rate is used, the constant β is introduced where:

$$\beta = \frac{dT}{dt} \tag{4}$$

The combination of Eqs. (1), (3) and (4) gives:

$$\frac{d\alpha}{dT} = \frac{A}{\beta}\exp\left(-\frac{E_a}{RT}\right)f(\alpha) \tag{5}$$

The Coats–Redfern integral method can be used to determine the parameters of the reaction rate constant, such as the activation energy and the pre-exponential factor. It assumes that the reaction model follows the *n*th-order reaction as follows:

$$f(\alpha) = (1-\alpha)^n \tag{6}$$

where $n = 1$ or $n \neq 1$.

Equation (5), thus, becomes:

$$\frac{d\alpha}{dT} = \frac{A}{\beta}\exp\left(-\frac{E_a}{RT}\right)(1-\alpha)^n \tag{7}$$

Rearrangement of Eq. (7) gives:

$$\frac{da}{(1-\alpha)^n} = \frac{A}{\beta}\exp\left(-\frac{E_a}{RT}\right)dT \tag{8}$$

Taking the integral of both sides gives:

$$\int_0^\alpha \frac{da}{(1-\alpha)^n} = \frac{A}{\beta}\int_0^T \exp\left(-\frac{E_a}{RT}\right)dT \tag{9}$$

For $n = 1$, Eq. (9) becomes:

$$-\frac{\ln(1-\alpha)}{T^2} = \frac{AR}{\beta E_a}\left[1-\frac{2RT}{E_a}\right]\exp\left(-\frac{E_a}{RT}\right) \tag{10}$$

For $n \neq 1$, Eq. (9) becomes:

$$\frac{1-(1-\alpha)^{1-n}}{T^2(1-n)} = \frac{AR}{\beta E_a}\left[1-\frac{2RT}{E_a}\right]\exp\left(-\frac{E_a}{RT}\right) \tag{11}$$

Since $\frac{2RT}{E_a}$ is negligibly small, it can be assumed as 0. Taking the natural log of both sides of the equation of Eqs. (10) and (11) gives a linear equation as follows:

For $n = 1$, Eq. (10) becomes:

$$\ln\left[-\frac{ln(1-\alpha)}{T^2}\right] = \ln\left[\frac{AR}{\beta E_a}\right] - \frac{E_a}{RT} \tag{12}$$

For $n \neq 1$, Eq. (11) becomes:

$$\ln\left[\frac{1-(1-\alpha)^{1-n}}{T^2(1-n)}\right] = \ln\left[\frac{AR}{\beta E_a}\right] - \frac{E_a}{RT} \tag{13}$$

Plotting the left side of Eqs. (12) and (13) against $\frac{1}{T}$ results in a slope of $-\frac{E_a}{R}$. Thus, the activation energy, E_a, of each stage can be determined. The linear fitting was solved using OriginPro software, and the E_a value with the highest correlation coefficient, R^2, at each individual peak region was chosen.

Determination of Reaction Model

The Šesták–Berggren function as proposed by Šesták and Berggren [18] provides an analytical form of mathematical expression where the majority of possible mechanisms can be described. The function that can best describe the reactions governed by the movement of phase boundaries, including simple nucleation, nucleation, nuclei growth and diffusion is:

$$f(\alpha) = \alpha^m(1-\alpha)^n[-\ln(1-\alpha)]^p \tag{14}$$

where *m*, *n* and *p* are the kinetic exponents representing processes controlled by diffusion, phase boundary reaction and nucleation, respectively.

Substitution of reaction model function, Eq. (14), into Eq. (5) gives:

$$\frac{d\alpha}{dt} = A\exp\left(-\frac{E_a}{RT}\right)\alpha^m(1-\alpha)^n[-\ln(1-\alpha)]^p \tag{15}$$

Equation (15) can be linearised by taking the nature log for both sides of the equation, resulting in Eq. (16) as follows:

$$\ln\left[\frac{d\alpha}{dt}\cdot\frac{1}{\exp\left(-\frac{E_a}{RT}\right)}\right] = \ln A + m\ln\alpha + n\ln(1-\alpha) + p\ln[-\ln(1-\alpha)] \tag{16}$$

Equation (16) can be expressed in the general form of multiple-linear equation as follows:

$$y = a + bx_1 + cx_2 + dx_3 \tag{17}$$

where $y = \ln\left(\frac{d\alpha}{dt}\cdot\frac{1}{\exp\left(-\frac{E_a}{RT}\right)}\right)$, $a = \ln A$, $b = m$, $c = n$, $d = p$, $x_1 = ln\ \alpha$, $x_2 = ln\ (1-\alpha)$, $x_3 = ln\ [-ln\ (1-\alpha)]$.

Since the activation energy was determined prior to determining the reaction mechanism, substitution of the activation energy of the respective stages gives an analytical solution for the parameters *A*, *m*, *n* and *p* by multiple-linear regression with OriginPro software. Proper combination of reaction mechanism exponents, *m*, *n* and *p*, should result in a plausible description of reaction mechanism. Table S1 in the Supporting Information shows the seven combinations of function and its suitability for the respective reaction. In the present study, the fitting of the model was assessed by the adjusted coefficient of

determination, i.e., adjusted, R^2, although numerous studies assessed the model fitting using R^2 value only. Consideration the large range of number of variables that are present in the functions listed in Table S1, adjusted R^2 should serve as a better criterion to assess the model fitting. The model fitting may be less accurate if the R^2 value is used instead given the presence of large number of fitted parameters that may give higher R^2 value.

Results and Discussion

Oil Palm Biomass Characterisation

The intrinsic properties of biomass play an important role in determining the most appropriate conversion process. Table 1 lists the proximate and ultimate analyses results of the oil palm biomass obtained in this work. The higher heating values (HHV) of five oil palm biomass are extracted from literature and tabulated in Table 1 for further correlation with the experimental results obtained in this study. The moisture content of oil palm biomass varies from 6.13 to 11.84%, where OPF has the highest moisture content followed by OPT, EFB, MF and PKS. The different moisture content of the oil palm biomass is related to the intrinsic structure of the plant and function. Typical thermochemical conversion requires feedstock moisture content of less than 10%, as the moisture content within biomass can have a direct impact on the useful energy that can be harvested [28] and, in some cases, the resultant products [29]. In combustion case, a significant portion of the heat generated from the process may be wasted to evaporate the moisture. High moisture content can also influence the composition of pyrolytic liquid [30] and promote secondary reactions in pyrolysis that promotes the formation of low molecular components (i.e., volatile organic products) [29]. Among the five biomass samples, OPF has the highest ash content of 4.65% while PKS has the lowest ash content of 1.86%. Lower ash content is generally desirable since the combustion of biomass with high ash content generally leads to significant slag formation that may cause blockage issue in the equipment during operation [22]. The HHV decreases in the order of PKS, MF, EFB, OPT and OPF [31]. Such trend correlates to the total fixed carbon and volatile content trend since these two components are the main contributors to HHV [32]. The volatile content and the fixed carbon content of these five biomass samples vary between 73.83 to 77.74% and 19.81 to 22.07%, respectively. The H/C and O/C ratios of the oil palm biomass can be calculated from the ultimate analysis results listed in Table 1. Among the five biomass samples, PKS has the lowest H/C and O/C ratio of 0.13 and 0.82, respectively. OPT, on the other hand, has the highest H/C ratio of 0.15 while OPF has the highest O/C ratio of 1.44. Biomass with low H/C and O/C ratio are generally preferred since high H/C and O/C ratios lead to lower heating value [33]. The sulphur and nitrogen contents of oil palm biomass are relatively low, which range from 0.04 to 0.16% and 0.20 to 1.65%, respectively. It is desirable to have these components in the lowest content possible since their presence in biomass during pyrolysis and combustion may lead to the formation of SO_x and NO_x emission. Sami et al. [33] also reported that biomass,

Table 1 Properties of oil palm biomass

Properties		OPT	PKS	OPF	MF	EFB
Proximate analysis[a]	(wt.%)					
Fixed carbon		21.94 ± 0.19	21.49 ± 0.45	21.39 ± 0.25	22.07 ± 0.31	19.81 ± 0.30
Volatile		74.78 ± 0.32	77.61 ± 0.34	73.83 ± 0.35	74.53 ± 0.23	77.74 ± 0.19
Ash		3.55 ± 0.17	1.86 ± 0.22	4.65 ± 0.27	3.24 ± 0.28	2.40 ± 0.16
Moisture		8.69 ± 0.19	6.13 ± 0.28	11.84 ± 0.22	6.78 ± 0.40	7.85 ± 0.37
Ultimate analysis[b]	(wt.%)					
C		39.90 ± 0.48	51.23 ± 0.18	38.62 ± 0.02	47.61 ± 0.02	49.78 ± 0.03
H		6.12 ± 0.16	6.47 ± 0.15	5.49 ± 0.22	6.54 ± 0.03	7.00 ± 0.12
N		0.20 ± 0.02	0.36 ± 0.02	0.32 ± 0.01	1.58 ± 0.02	1.65 ± 0.04
S		0.12 ± 0.01	0.04 ± 0.00	0.10 ± 0.00	0.16 ± 0.01	0.15 ± 0.01
O[c]		53.66 ± 0.61	41.90 ± 0.01	55.46 ± 0.23	44.11 ± 0.04	41.42 ± 0.12
H/C ratio		0.15	0.13	0.14	0.14	0.14
O/C ratio		1.34	0.82	1.44	0.93	0.83
HHV [31]	(MJ/kg)	17.47	20.09	15.72	19.06	18.88

[a] Weight percent as received

[b] Weight percent in dry basis

[c] Calculated by differences

in general, have negligible sulphur and nitrogen content relative to coal, which makes it a more environmentally sustainable thermochemical conversion feedstock.

Thermograms Analysis

Figure 1a,c and Fig. 1b,d display the thermogravimetric (TG) and derivative thermogravimetric (DTG) profiles of OPT, PKS, OPF, MF and EFB obtained at a 10 °C/min heating rate under non-oxidative (pyrolysis) condition and oxidative (combustion) condition, respectively. Figures 2 and 3, on the other hand, show a representative deconvolution process for the pyrolysis and combustion of the five oil palm biomass, respectively. Their global DTG peaks were deconvoluted into their individual peaks that represent different reaction stages. The total number of the individual peaks and the location of these peaks vary depending on the biomass sample and the reaction condition. The pyrolysis of oil palm biomass in this work is postulated to occur through three main regimes based on the TG profile, i.e., (1) surface-bound moisture and light volatile removal (30–140 °C); (2) devolatilisation of hemicellulose and cellulose (140–420 °C); and (3) slow devolatilisation of lignin (> 380 °C) (Table 3). The combustion of oil palm biomass is also postulated to take place through three main regimes, i.e., (1) surface-bound moisture and light volatile removal (30–140 °C); (2) devolatilisation of hemicellulose and cellulose (140–390 °C); and (3) char combustion (> 370 °C) (Table 4). Although the first and second regimes in both pyrolysis and combustion cases have the same phenomena origins, the third regimes in both cases represent two different phenomena. Moreover, the second regime in pyrolysis case appears to have slightly higher terminal temperature than that in combustion case. To match the individual peaks to their respective regimes and to simplify the following discussion, the DTG peaks in Fig. 1c,d are classified into several peaks, i.e., Peaks 1, 2.1, 2.2, 2.3, 3.1 and 3.2. In these peak labels, the initial number indicates the regime number where the peak is located while the subsequent number (in Peak 2 case for pyrolysis and Peak 3 case for combustion) implies the sequence where the peak appears within the temperature range for the 2nd regime. In OPT pyrolysis case (Fig. 2a), for example, the first peak (Peak 1) corresponds to the moisture and light volatile release. The second regime, however, consists of two different peaks, i.e., Peak 2.1 that we attribute to hemicellulose decomposition and Peak 2.2 that we ascribe to cellulose decomposition. This is since the latter occurs at higher temperature than the former, which is consistent with the fact that cellulose decomposition occurs at higher

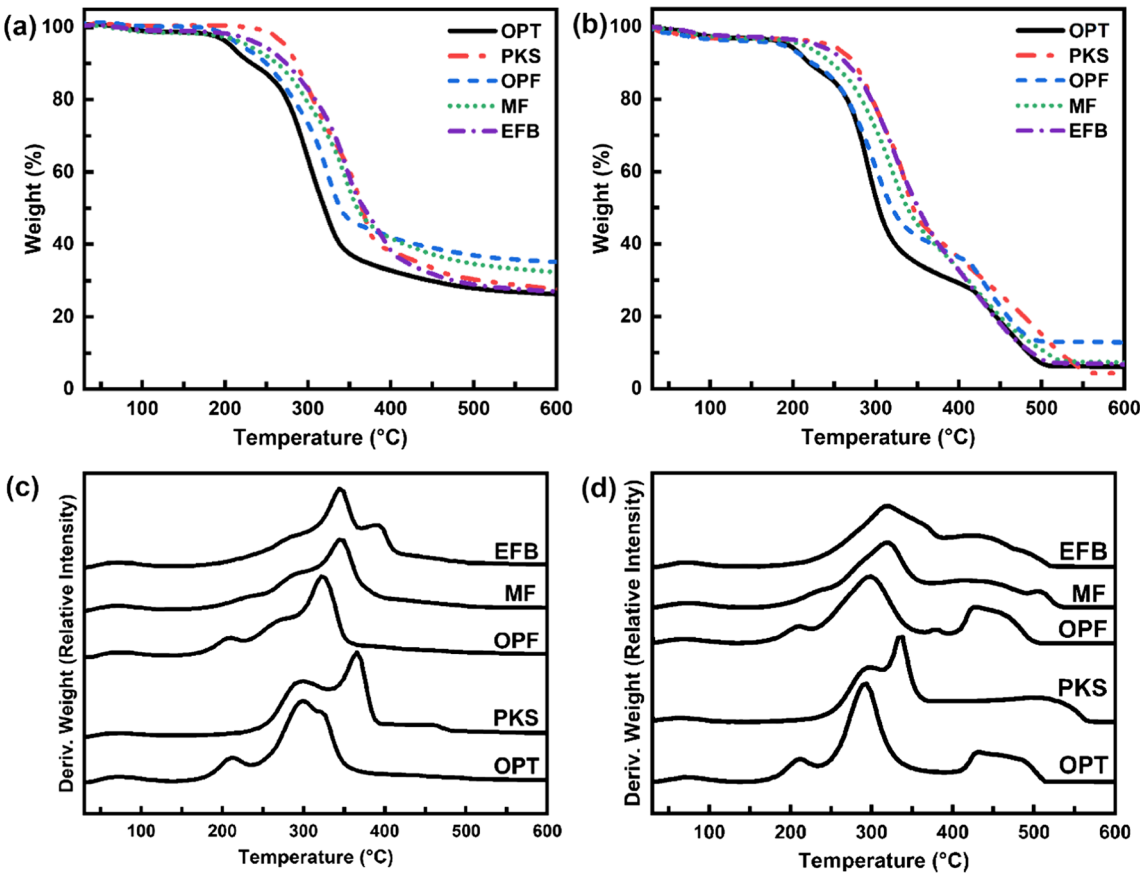

Fig. 1 Thermogravimetric profiles of oil palm biomass under (**a**) non-oxidative condition and (**b**) oxidative condition, and the respective DTG profiles under (**c**) non-oxidative condition and (**d**) oxidative condition

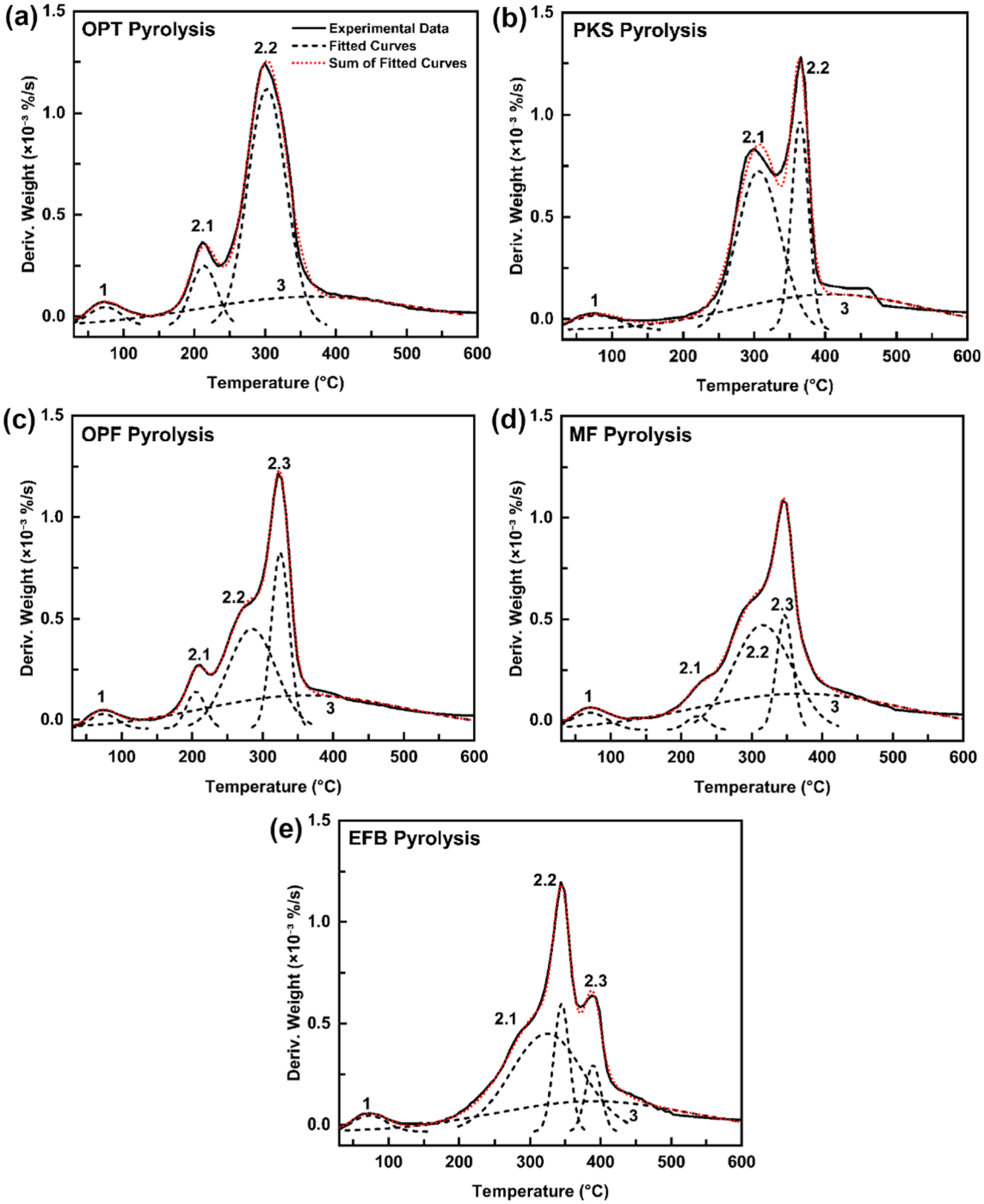

Fig. 2 Deconvolution of the global DTG peaks for pyrolysis of (**a**) OPT, (**b**) PKS, (**c**) OPF, (**d**) MF and (**e**) EFB into their individual peak components

temperature than the hemicellulose decomposition [14]. While hemicellulose has irregular branching and random amorphous structure, cellulose has unbranched crystalline structure linked by glycosidic bonds, which is more stable than that of hemicellulose [34, 35]. The flatter bottom peak that extends across the whole temperature range, on the other hand, represents lignin decomposition, which is defined as Peak 3. The decomposition of lignin occurs in parallel with the other reactions once the temperature was raised to above room temperature, the extent of which was marginal with respect to the other reactions until the temperature reached 370 °C, beyond which it became the sole reaction (Fig. 2). For simplicity's sake, the onset temperature of regime 3 is taken as 380 °C (in pyrolysis case). OriginPro's multiple peak fitting tool was used to determine the characteristics of the individual peaks, i.e., the starting temperature, the final

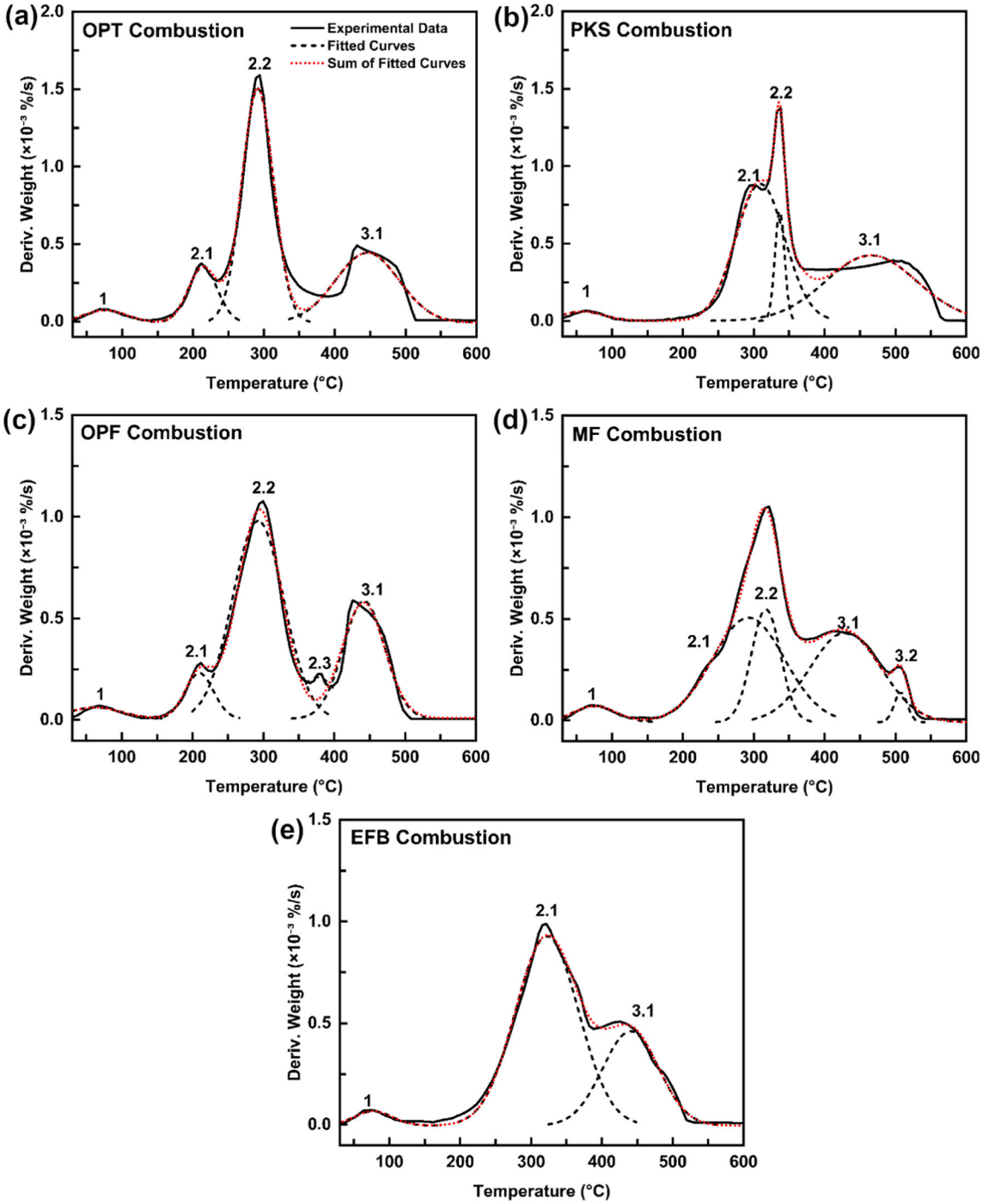

Fig. 3 Deconvolution of the global DTG peaks for combustion of (**a**) OPT, (**b**) PKS, (**c**) OPF, (**d**) MF and (**e**) EFB into their individual peak components

temperature and the peak temperature, for all the DTG profiles obtained from pyrolysis and combustion of the five biomass samples; the results of which are listed in Tables 3 and 4, respectively.

TG profiles for pyrolysis and combustion of all five samples (Fig. 1a,b) reveal that the decomposition rate from 140 to 200 °C was low where no significant weight loss was observed. Increasing temperature above 200 °C led to the substantial weight loss for all biomass samples except for PKS, the onset temperature of which was higher, i.e., 250 °C (Fig. 1a,b). Such 50 °C higher onset pyrolysis and combustion temperature for PKS relative to the other oil palm biomass is consistent with the report of Luangkiattikhun et al. [11].

As discussed previously, the thermal decomposition of hemicellulose, cellulose and lignin occurs at different temperature range and decomposition rate. Several works are

available that discuss the decomposition temperature ranges of hemicellulose, cellulose and lignin [25, 35, 36]. Stefanidis et al. [35] reported that the pyrolysis of hemicellulose, cellulose and lignin occurs at 200–320, 280–360, and 140–600 °C, respectively. Kai et al. [36] and López-González et al. [25], on the other hand, reported that during combustion, hemicellulose, cellulose and lignin decomposition takes place at 195–368, 244–413, and 138–700 °C, respectively. Subsequently, combustion of char takes place at 360 °C onwards. Sharp distinction in temperature range of different decomposition stage is normally not possible given the overlapped temperature ranges where any two or three reactions occur in parallel. These reported temperature ranges are in close agreement with the temperature ranges displayed in Tables 3 and 4.

In the pyrolysis of five oil palm biomass samples, Peak 2.1 in OPT, PKS and EFB cases and Peaks 2.1 and 2.2 in OPF and MF cases are attributed to hemicellulose decomposition based on their onset temperatures and DTG peak shapes (Table 3 and Fig. 2a–e). For example, Peak 2.2 in OPT case is attributed to cellulose decomposition instead of hemicellulose decomposition despite its quite low-onset temperature of 235 °C, which overlaps with hemicellulose decomposition. This is since cellulose decomposition generally occurs at the highest decomposition rate as suggested by the well-defined maximum peak shape of Peak 2.2 in OPT case (Fig. 2a) [25]. Likewise, Peak 2.1 in the combustion of OPT, PKS, OPF, MF and EFB is ascribed to hemicellulose decomposition (Table 4 and Fig. 3a–e). Our data in Tables 3 and 4 indicate that hemicellulose decomposition takes place from 140 to 331 °C and from 140 to 313 °C in pyrolysis case and combustion case, respectively.

Following hemicellulose decomposition is cellulose decomposition. In the pyrolysis case, cellulose decomposition is represented by Peak 2.2 in OPT and PKS cases, Peak 2.3 in OPF and MF cases, and Peaks 2.2 and 2.3 in EFB; the peak temperature range of which lies between 235 and 435 °C. Similarly, cellulose decomposition in combustion case is represented by Peak 2.2 in OPT, PKS and MF cases and Peaks 2.2 and 2.3 in OPF case. It is worth noting that only one peak arises in the temperature range for second regime of combustion for EFB, i.e., Peak 2.1 (Fig. 3e), which makes assigning this peak to single-component decomposition invalid. Closer inspection to second regime in the pyrolysis and combustion of all five biomass reveals that stronger overlapping tendency between the peaks that represents hemicellulose decomposition and cellulose decomposition in EFB cases (Tables 3 and 4 and Fig. 2e and Fig. 3e) relative to OPT, PKS, OPF and MF cases (Tables 3 and 4 and Figs. 2a–d and 3a–d), which could be attributed to the presence of relatively larger potassium (K) content in EFB [37–39].

The last peaks in the third regime correspond to lignin decomposition and/or char oxidation. Peak 3.1 in the pyrolysis of five oil palm biomass comes from lignin decomposition (Table 4 and Fig. 2a–e) whereas Peaks 3.1 and 3.2 in the combustion of five oil palm biomass arise from simultaneous lignin decomposition and char oxidation. The onset temperature for lignin decomposition in pyrolysis and combustion is 380 and 372 °C, respectively. As discussed previously, lignin decomposition started immediately after the moisture removal was complete at a relatively low rate and over a wide temperature range given the thermally stable structure of lignin [14]. The higher onset temperatures for pyrolysis and combustion of PKS relative to those of the other biomass reported elsewhere (Fig. 1a,b) reflects the higher lignin content in PKS (Table 2) [40–42]. Such high lignin content has been reported as the contributing factor behind the shifting of the hemicellulose and cellulose decompositions to higher temperature range [43]. Lignin generally undergoes slow decomposition process where char is formed as the product [24]. The presence of char together with oxygen in combustion leads to the conversion of char into ash. In both pyrolysis and combustion cases, negligible weight loss is observed above 600 °C. Following the heating to 1000 °C, TG profiles reveal that the final char content in pyrolysis of five oil palm biomass varies between 17 and 23% (Fig. S1), while the final ash content in combustion of five oil palm biomass varies between 4.7 and 7% (Fig. S2).

Kinetic Analysis

The kinetic parameters of the pyrolysis and combustion of five oil palm biomass were determined using the Coats–Redfern integral method and the Šesták–Berggren reaction model by model-fitting method. The Coats–Redfern integral method was initially used to determine the activation energies, E_a, and the reaction orders, n. The resultant activation energies were then substituted into the Šesták–Berggren reaction function to obtain the kinetic exponents m, n and p which represent processes controlled by diffusion, phase boundary reaction and nucleation, respectively. The highest correlation coefficient, R^2, was used to evaluate the suitability of the reaction order in the Coats–Redfern integral method and the reaction mechanism in the Šesták–Berggren reaction function, respectively.

Table 2 Composition of major components in oil palm biomass obtained from literature

Biomass	Composition (%)			
	Hemicellulose	Cellulose	Lignin	Extractives
OPT [40]	17.74	45.81	24.49	11.96
PKS [41]	22.93	20.92	51.23	4.92
OPF [42]	16.69	56.03	20.48	4.40
MF [41]	19.36	38.90	33.11	8.63
EFB [41]	35.27	39.07	22.84	2.82

Activation Energy

Tables 3 and 4 present the resultant activation energies and reaction orders of the Coats–Redfern integral method that provides the best fit into the pyrolysis and the combustion of oil palm biomass, respectively. An example of the linear regression graph for the pyrolysis of OPT at Peak 2.1 is shown in Fig. S3 in the Supporting Information. The average correlation coefficient, R^2, is 0.9645. Since Peak 1 represents moisture removal, the activation energy in this first regime was not determined. The kinetics of this study will be evaluated based on decomposition range of the three major components of oil palm biomass, i.e., hemicellulose, cellulose and lignin, as discussed in the previous section (Figs. 2 and 3). The activation energy is best pictured as the minimum energy required to start a reaction; hence, high activation energy indicates low reactivity of the thermal decomposition of oil palm biomass. The reaction order, n, correlates to the complexity of the reaction, where low n value corresponds to simple reaction, whereas higher n value corresponds to a complex reaction.

The activation energies of oil palm biomass pyrolysis and combustion during hemicellulose decomposition were lower (i.e., 23.07–84.10 kJ/mol) relative to cellulose decomposition (i.e., 45.2–178.11 kJ/mol) (Tables 3 and 4). This is since hemicellulose has a linear polymeric structure with weakly linked sites that is easily broken, thus requiring lower amount of energy [44]. The activation energies for cellulose decomposition vary to larger extent relative to those for hemicellulose decomposition. This is consistent with the higher reaction orders, n, for cellulose decomposition (i.e., maximum 5) relative to that for hemicellulose decomposition (i.e., maximum 2); both of which indicate the occurrence of overlapping reactions during cellulose decomposition due to the presence of inorganic mineral content in oil palm biomass [14]. Moreover, among five oil palm biomass, the activation energy of PKS is the highest in hemicellulose decomposition for both pyrolysis case and combustion case (Peak 2.1 in Tables 3 and 4), which suggests low reactivity. PKS has been known to have dense surface and rigid cell walls that require high energy input to decompose [41].

Lignin decomposition in pyrolysis exhibits an order of reaction, n, that varies between 5 and 6 with activation energy that varies from 34.94 to 122.24 kJ/mol. PKS displays the highest activation energy of 122.24 kJ/mol, while OPF exhibits the lowest at 34.94 kJ/mol. Highest activation energy for PKS is in accord with its highest lignin content (Table 2). Lignin is more difficult to decompose than hemicellulose and cellulose given its cross-linked polymeric structure [36]. Char oxidation in combustion, which starts at almost similar temperature to lignin decomposition in pyrolysis, on the other hand, displays an order of reaction that varies between 1 and 1.5, while activation energy varies from 23.75 to 52.77 kJ/mol. The presence of oxygen can promote the formation of volatiles, which allows char oxidation to take place with lower energy barrier [34].

Reaction Mechanism

To determine the reaction mechanism, the Šesták–Berggren reaction model was used to find the exponents of the function, m, n and p. The reaction function that has the best fit was chosen based on the adjusted R^2 value. Functions (1) and (3) (Table S1) are not applied here as their applicability to describe particular reaction mechanisms has not been confirmed experimentally [18]. In cases where the adjusted R^2 values are identical (i.e., ± 0.1) for all seven functions, the function model that best describes various stages of the reaction is chosen. Tables 5 and 6 list the resultant parameters of the Šesták–Berggren function for the different individual peaks deconvoluted from the global DTG peaks for pyrolysis and combustion of the five oil palm biomass. The kinetic parameters, m, n and p, are associated with diffusion, phase boundary reaction and nucleation, respectively. Higher value of the kinetic parameter normally indicates the domination of a particular reaction mechanism associated with that parameter. For instance, in a case where m is higher than n and p, diffusion prevails over phase boundary reaction and nucleation.

The pyrolysis and combustion of five oil palm biomass are best correlated using Function (4), which suggests the combined role of phase boundary and nucleation reaction. This is evident from the presence of only 2 kinetic parameters, i.e., n

Table 3 Activation energies of the Coats–Redfern model for the pyrolysis of five oil palm biomass

Peak biomass	2.1			2.2			2.3			3		
	n	E_a (kJ/mol)	R^2	n	E_a (kJ/mol)	R^2	n	E_a (kJ/mol)	R^2	n	E_a (kJ/mol)	R^2
OPT	1	42.59	0.9710	2.8	80.77	0.9754				6	62.14	0.9916
PKS	1	84.10	0.9865	3	136.44	0.9770				5	122.24	0.9926
OPF	1	52.31	0.9738	1	40.08	0.9957	5	147.80	0.9697	5	34.94	0.9724
MF	1	23.07	0.9232	1	43.22	0.9970	5	132.41	0.9730	5	51.20	0.9934
EFB	2	32.48	0.9440	1	53.38	0.9930	5	178.11	0.9801	5	56.95	0.9495

Table 4 Activation energies of the Coats–Redfern model for the combustion of five oil palm biomass

Peak biomass	2.1			2.2			2.3			3.1			3.2		
	n	E_a (kJ/mol)	R^2	n	E_a (kJ/mol)	R^2	n	E_a (kJ/mol)	R^2	n	E_a (kJ/mol)	R^2	n	E_a (kJ/mol)	R^2
OPT	1	36.94	0.9677	5	109.81	0.9619				1	32.13	0.9238			
PKS	1	51.47	0.9192	5	139.33	0.9751				1	27.39	0.7996			
OPF	1	29.28	0.9428	3	64.62	0.9847	5	45.20	0.9967	1.5	52.77	0.9772			
MF	1	23.34	0.9053	2.9	69.57	0.9930				1	23.75	0.9861	1	53.32	0.9693
EFB	1	44.52	0.9846							1	36.71	0.9809			

and p in this function. In the pyrolysis and combustion of the five oil palm biomass, phase boundary reaction dominates the hemicellulose and cellulose decompositions (i.e., Regime 2) as denoted by larger values of n relative to p (Peaks 2.1, 2.2 and 2.3 in Tables 5 and 6). With temperature rise, nonetheless, as hemicellulose decomposition shifts into cellulose decomposition, the disparity between the n and p values is lessened although the value of n is still larger than p. This indicates the increasing role of nucleation reaction with increasing temperature, i.e., during cellulose decomposition. Unlike hemicellulose and cellulose decomposition cases, lignin decomposition in pyrolysis and char oxidation in combustion of oil palm biomass are dominated by nucleation reaction except char oxidation of PKS and MF that is jointly controlled by both phase boundary and nucleation simultaneously.

Mass Spectrometry Analysis

The gas product distributions of the pyrolysis and combustion of five oil palm biomass were evaluated using mass spectrometry (MS). The ion current of the mass spectrum profile is plotted against temperature (Figs. 4 and 5). Here, we focus only on the thermal release profiles of permanent gases (hydrogen (H_2) and carbon dioxide (CO_2)), light hydrocarbon (methane or CH_4), and water (H_2O), which are represented by mass spectra profiles of m/z = 2, 28, 44, 16 and 18, respectively. The thermal release profiles of nitrogen oxides (NO_x) and sulphur oxides (SO_x) are also presented and discussed to identify the primary temperature ranges where these gases are emitted during pyrolysis and combustion.

The main gases emitted from the pyrolysis of oil palm biomass are H_2O and CH_4, whereas for combustion case, the main gases emitted are CO_2, H_2O and CH_4. Majority of the gases are emitted between 250 and 600 °C (Figs. 4 and 5).

In both pyrolysis and combustion cases, H_2O signal starts to appear at the onset of heating as a result of moisture removal from the samples (Figs. 4a and 5a). A well-defined peak comes out between 300 and 450 °C, which originates from the release of H_2O above 300 °C from the depolymerisation of cellulose that involves dehydration of reaction in combustion and pyrolysis [45, 46]. Moreover, since lignin degradation spans across the whole temperature range tested, the release of water beyond 380 °C is also observed that can be attributed to the decomposition of monomer of lignin (i.e., guaiacol → o-quinone-methide + H_2O) [45].

CH_4 emission occurs in two stages at two different temperature ranges, i.e., 280–440 and 480–640 °C in pyrolysis case and 270–410 and 420–630 °C in combustion case (Figs. 4b and 5b). The first stage in both pyrolysis and combustion cases can be attributed to the cracking of methyl and methylene that are present in hemicellulose and cellulose while the second stage comes from the decomposition of lignin [47].

Major formation of CO_2 is detected at 280–450 °C in pyrolysis case and at 280–630 °C in combustion case (Figs. 4c and 5c), both of which can be attributed to the cracking and reforming of carbonyl and carboxyl groups in cellulose between 280 and 400 °C [48]. The extended higher temperature

Table 5 Kinetic parameters of the Šesták–Berggren reaction model for pyrolysis of oil palm biomass

Peak	2.1			2.2			2.3			3		
Biomass	n	p	Adj. R^2	n	p	Adj. R^2	n	p	Adj. R^2	n	p	Adj. R^2
OPT	52.84	3.89	0.9748	6.18	2.12	0.9593				39.38	60.55	0.9933
PKS	4.97	0.45	0.9201	10.76	7.61	0.9284				65.19	124.16	0.9762
OPF	53.02	2.45	0.9602	5.06	1.01	0.7906	12.83	5.50	0.9476	37.48	48.63	0.9874
MF	58.92	4.21	0.9545	5.55	1.10	0.8342	12.56	5.51	0.9808	32.43	39.50	0.9983
EFB	12.17	1.48	0.8867	4.24	1.61	0.8237	24.32	24.90	0.9910	41.71	70.02	0.9948

Table 6 Kinetic parameters of the Šesták–Berggren reaction model for combustion of oil palm biomass

Peak biomass	2.1			2.2			2.3			3.1			3.2		
	n	p	Adj. R^2	n	p	Adj. R^2	n	p	Adj. R^2	n	p	Adj. R^2	n	p	Adj. R^2
OPT	61.91	4.72	0.9699	11.12	3.34	0.9805				5.05	10.21	0.8071			
PKS	9.57	1.56	0.9975	22.64	10.25	0.9838				0.07	−0.63	0.9790			
OPF	86.61	5.83	0.9829	7.80	1.88	0.9537	212.19	221.89	0.9131	11.61	18.32	0.8499			
MF	57.22	4.88	0.9438	5.37	1.03	0.9820				1.47	1.44	0.9980	12.30	40.84	0.9206
EFB	3.45	0.78	0.9950							1.62	1.82	0.9260			

range for the combustion case is consistent with the fact that CO_2 was also generated during the char oxidation above 370 °C, which overlaps with the previous cracking and reforming process [27]. Such char oxidation process is substantiated by the additional weight loss above 400 °C on the TG profile for combustion case (Fig. 1b), which is absent in the TG profile for pyrolysis case (Fig. 1a).

Unlike their pyrolysis counterparts where only a single peak is observed (Fig. 4a,c), two distinct peaks are present on the H_2O and CO_2 evolution profiles obtained from the combustion of OPT, OPF and PKS in the temperature ranges of 280–450 and 450–580 °C (Fig. 4a,c). The second peak in these profiles arisen from the oxidation of hydrocarbon that was produced at temperature range of 450–580 °C [47]. The two peaks that are present in H_2O and CO_2 evolution profiles from the combustion of MF and EFB overlap with a distinctive shoulder at 400 and 430 °C, respectively.

Dominant release of H_2 in pyrolysis of the five oil palm biomass that starts at 600 °C (Fig. 4d) correlates with the secondary release of CO_2 (Fig. 4c), which can possibly be explained by self-gasification of char according to Eq. (18) [23].

$$C + H_2O + \frac{1}{2}O_2 \rightarrow CO_2 + H_2 \tag{18}$$

Such self-gasification of char is clearly absent in combustion case (Fig. 5c,d). This is since char was directly oxidised in the presence of excess oxygen. Likewise, the char retained in pyrolysis condition may undergo self-gasification as temperature increases.

For both pyrolysis and combustion cases, the temperature-dependent release profile of gas product with m/z of 28 can be attributed to CO or N_2. Figures 4e and 5e display continuous flat profile over the whole tested temperature range; most likely coming from N_2 that was always present in both pyrolysis and combustion experiments. Although literature reported the possibility of CO generation mainly from the Boudouard reaction [49], the trends observed from Fig. 4e and Fig. 5e do not indicate the occurrence of such phenomena.

Nitrogen oxides and sulphur oxides are known for their harmful effect to the environment. Nitric oxide (NO), nitrogen dioxide (NO_2) and sulphur dioxide (SO_2) emissions from the pyrolysis and combustion are represented by the gas product releases with m/z of 30, 46 and 64, respectively. Although the mass spectra m/z 30 can be associated with the release of C_2H_6 and CH_2O, presence of oxygen can promote the formation of NO and NO_2 during pyrolysis and combustion [50]. In addition, the ion intensities emitted from m/z 30 are relatively low, which is consistent with the low nitrogen content in the biomass (Table 1). However, the possibility for the interference of signals from various compounds with the a.m.u. of 30 to the m/z 30 profiles shown in Figs. 4f and 5f cannot be completely ruled out. The formation of nitric oxide and nitrogen dioxide was more intense in combustion case relative to pyrolysis case. In pyrolysis case, nitric oxide and nitrogen dioxide were produced mainly between 220 and 450 °C (Fig. 4f,g). In combustion case, nonetheless, two stage release took place between wider temperature range of 220–630 °C (Fig. 5f,g). The secondary release of nitric oxide and nitrogen dioxide is associated with the oxidation of residual nitrogen in char [51]. SO_2 was generated mainly between 300 and 600 °C during pyrolysis and between 280 and 550 °C during combustion (Figs. 4h and 5h). Among these three harmful gases, NO appears to be produced in the largest amount followed by NO_2 and, then, SO_2 (i.e., $NO > NO_2 > SO_2$). This is consistent with the elemental analysis results (Table 1), which reveals the lower sulphur content relative to nitrogen content in all five oil palm biomass.

Practical Implications

Thermochemical conversion technologies can convert low-value biomass into value-added products, such as bio-char, bio-oil, syngas, heat and electricity. Efficient thermochemical conversion process requires knowledge of the biomass characteristics and their thermal decomposition behaviour. Generally, an ideal biomass feedstock should be available in abundant amount, provide high conversion yield, have low energy penalty, have low operation and maintenance cost,

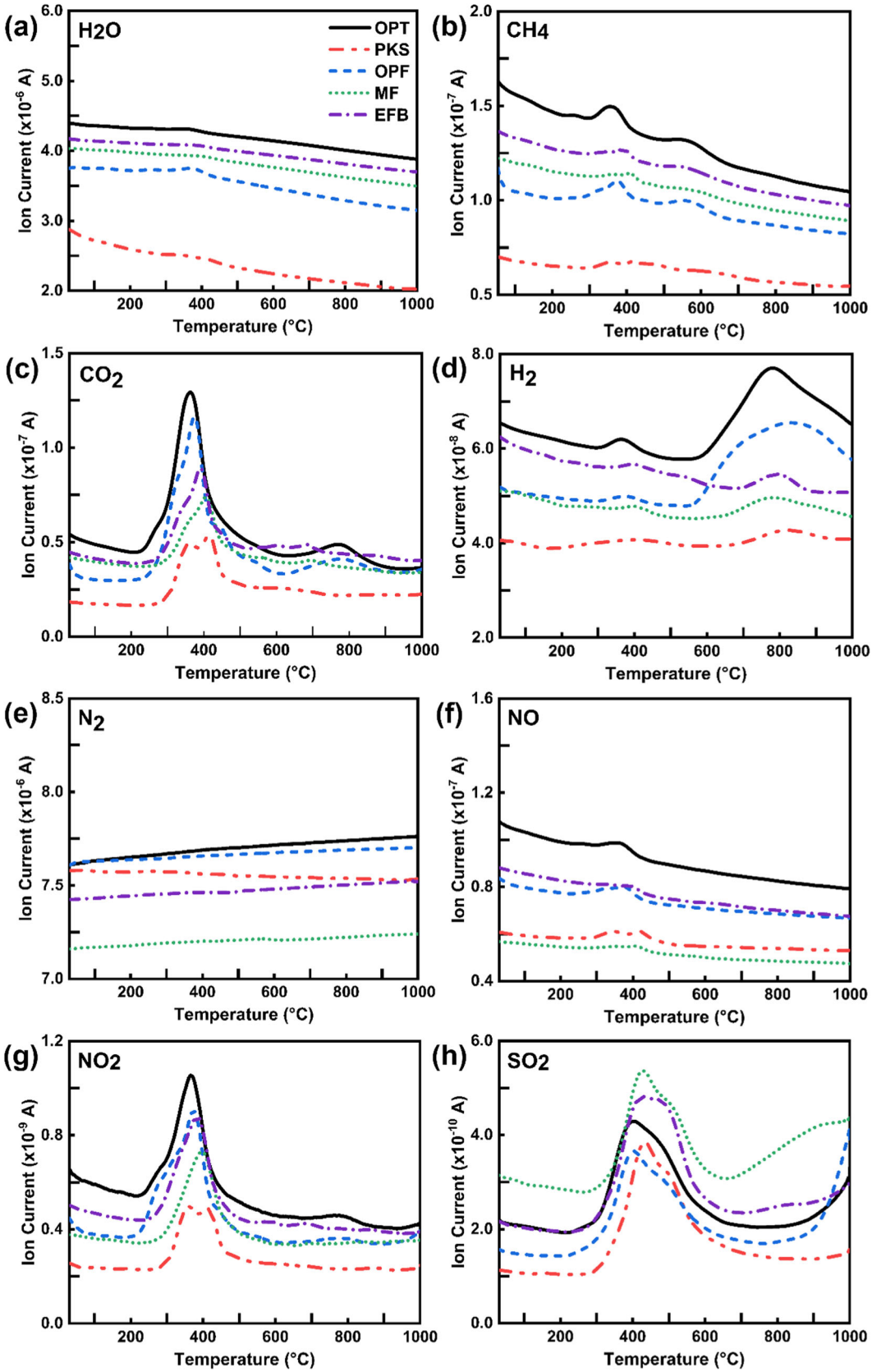

Fig. 4 Mass spectra for the gas products of pyrolysis of the oil palm biomass: (**a**) H_2O, (**b**) CH_4, (**c**) CO_2, (**d**) H_2, (**e**) N_2, (**f**) NO, (**g**) NO_2 and (**h**) SO_2

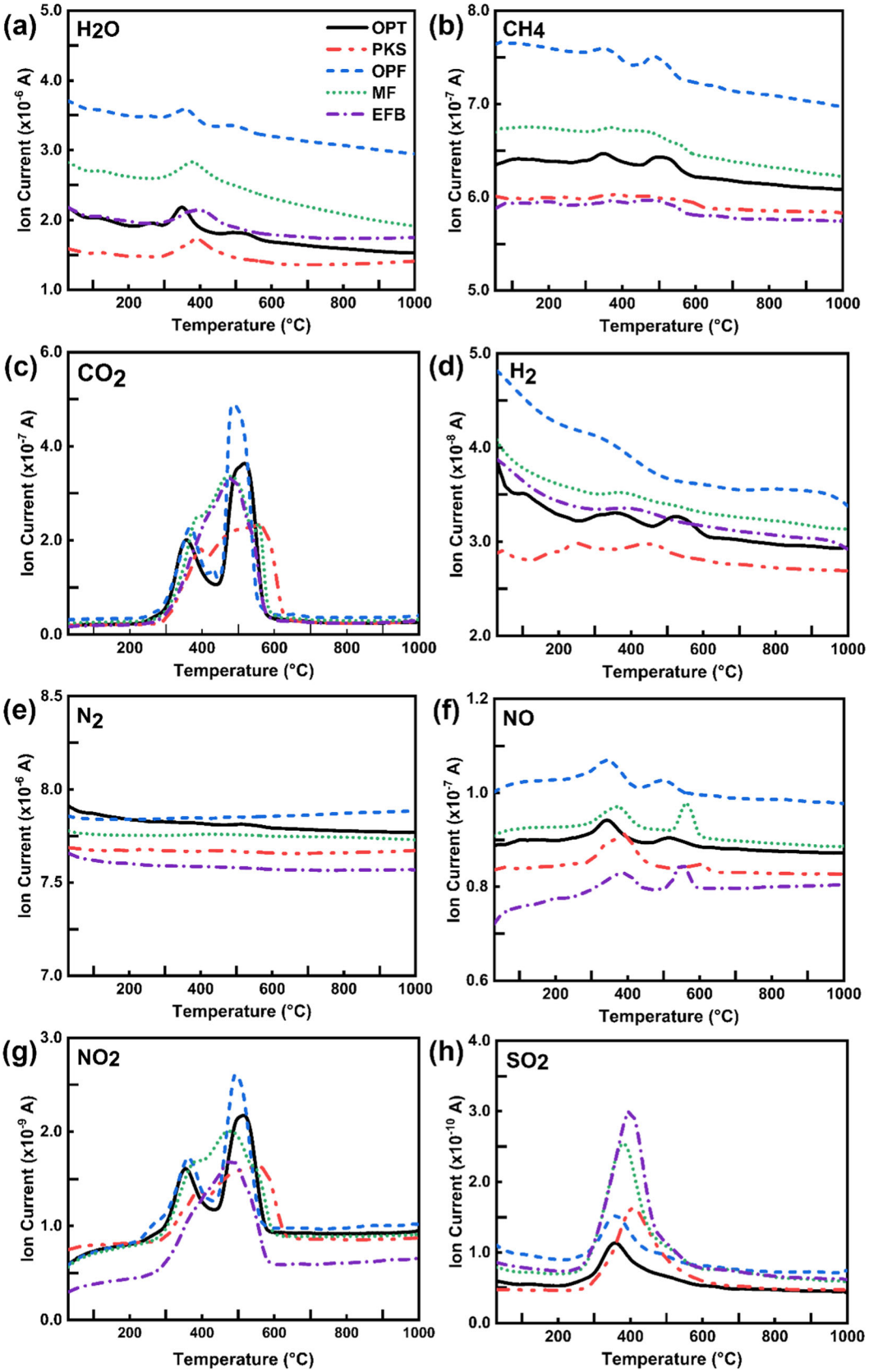

Fig. 5 Mass spectra for the gas products of combustion of the oil palm biomass: (**a**) H_2O, (**b**) CH_4, (**c**) CO_2, (**d**) H_2, (**e**) N_2, (**f**) NO, (**g**) NO_2 and (**h**) SO_2

and contain low undesirable components that may affect negatively the process and product quality [22].

For thermochemical conversion processes, such as pyrolysis, combustion, and gasification, it is desirable to have biomass feedstock with high HHV, low moisture content, low ash and alkali metal content and low pollutant gas emission. Depending on the desired product, different operating conditions can result in different product constituents. Pyrolysis can be categorised into three main categories, i.e., slow pyrolysis, fast pyrolysis and flash pyrolysis. Their main differences lie in their heating rates and reactor residence time.

Slow pyrolysis is performed at low heating rate (i.e., 0.1–1 °C/s) and typically aims to generate solid bio-char as the main product [15, 52]. Hence, it is desirable to utilise feedstock with high lignin content and low ash content since lignin is the main contributor for char formation, while ash can hamper fixed carbon formation in bio-char [53]. Among the five oil palm biomass, PKS is the most suitable slow pyrolysis feedstock, followed by MF and EFB. Lignin content of PKS is the highest among the five biomass (i.e., 51.23%) with moisture content of 6.13% while MF and EFB have lower ash content and higher HHV compared to OPT and OPF. The drawback of using MF and EFB as feedstock instead of PKS lies in their lower yield of bio-char given their lower lignin content relative to PKS. MF and EFB, nonetheless, require lower energy to start the reaction relative to PKS, which may translate to more economic process. Among the various reactors available for slow pyrolysis, fixed-bed reactor is recommended since this reactor can accommodate various biomass feed size (small or large), thus removing the need for comminution before reaction. Fixed bed reactor allows higher carbon content to be retained in the final product, thus maximises the production of solid bio-char [15]. Our observation on the DTG thermal behaviour and MS results suggests that bio-char production via slow pyrolysis using PKS, MF and EFB is best operated below 400 °C where most volatiles were released. Relative to these three biomass, OPT and OPF are less suitable for slow pyrolysis due to their low lignin content and low HHV. Fermentation is perhaps a better conversion pathway for OPT and OPF given their high cellulose, low lignin content and high moisture content [22].

Fast pyrolysis is typically implemented at higher heating rate (i.e., 10–200 °C/s) than slow pyrolysis and temperature between 400 and 550 °C with bio-oil as the target product [52]. MF and EFB are considered as more suitable feedstocks relative to OPT, PKS and OPF for bio-oil production since MF and EFB have lower NO and NO_2 emission and high HHV. In addition, bio-oil is mainly derived from cellulose that is depolymerised into condensable organic compounds-containing volatiles [45]. Hence, the high cellulose content in MF and EFB makes them suitable materials for bio-oil production. The low energy requirement and the high reactivity of OPT and OPF are desirable properties for bio-oil production. However, the high moisture content (i.e., > 10% water content) and hygroscopic nature of OPF and OPT can lead to high water content in the bio-oil, which decreases the HHV of the bio-oil [28]. Depolymerisation and volatilisation of PKS furthermore occur at relatively high temperature (i.e., above 250 °C) and requires higher energy input. Based on these arguments, the potential of using OPT, OPF and PKS for bio-oil production, is less attractive relative to MF and EFB. Bubbling fluidised bed (BFB) reactor is recommended for fast pyrolysis process as BFB can generate up to 70–75% of bio-oil from the biomass on dry basis. The generated char can be separated rapidly, thus reducing the char accumulation issue in the reactor [15]. Efficient operation of BFB, nonetheless, relies upon efficient heat transfer process, which requires the use of less than 3 mm biomass feed particles [15]. The fibrous nature of MF and EFB can be advantageous for pre-processing requirements of BFB.

Unlike pyrolysis, combustion is performed at oxidising atmosphere and above 700 °C mainly to produce heat and electricity [8]. Most palm oil mills currently utilise their oil palm biomass onsite as boiler fuel to generate steam and electricity for the mills' operation [13]. For combustion application, high HHV is a desirable characteristic for fuel material since more energy can be released per unit weight. Among the five oil palm biomass examined in this work, PKS shows the best potential as feedstock for combustion given its high HHV and low CO_2, NO, NO_2 and SO_2 emissions. In addition, the low ash content of PKS is anticipated to minimise the operating issues related to fouling, scaling and corrosion of the reactor [22]. MF is the second-best feedstock for combustion after PKS. Combustion of MF however may contribute to emissions of NO, NO_2 and SO_2 as revealed by its MS profile (Fig. 4f–h). Although EFB has high HHV and low activation energy, which are desirable characteristics for combustion, its high SO_2 emission may require additional post-treatment equipment. In addition, EFB also contains high potassium (K) and silica (Si), which may cause the fouling of the equipment and lower boiler efficiency [22, 54]. OPT and OPF are the least attractive feedstock for combustion given their high moisture content, which may result into longer ignition time and lower combustion efficiency relative to PKS. Various types of combustion systems are available that have different specifications and requirements. For practical purpose, it is desirable to have combustion furnace that is robust and can accommodate different types of feedstock. Among the conventional combustion systems available, grate furnace, particularly moving grate furnace, is recommended for oil palm biomass combustion since it requires low investment cost and can tolerate feedstocks with high ash and moisture content [55].

Gasification for syngas production (i.e., CH_4, H_2, CO and CO_2) by air, oxygen or steam is another pathway for oil palm biomass utilisation [56]. From their MS profiles (Fig. 4c,d),

OPT and OPF emitted significant amount of H_2 and CO_2 above 600 °C due to the self-gasification, which makes them a suitable material for hydrogen fuel production via gasification [57]. Nipattummakul et al. [58] investigated the steam gasification of OPT, mangrove wood, paper waste, food waste and polystyrene using a batch reactor. They reported that OPT exhibited the best gasification performance in terms of syngas yield, energy yield and apparent thermal efficiency (i.e., syngas energy yield per solid fuel energy yield), which was attributed to the high volatile matter of OPT and high reactivity of the OPT char. Atnaw et al. [59] studied the performance of OPF as a fuel for downdraft gasification. They found that the gasification of OPF at optimum parameters resulted in highest apparent thermal efficiency of 70.2% and carbon conversion of 93%. The high carbon conversion of OPF reflects the high reactivity of OPF and leads to the almost complete conversion of the initial carbon content of OPF into gaseous product and reduced tar formation.

Three different types of commercial gasifiers are present, i.e., fixed or moving bed, fluidised bed and entrained bed [60]. The operating capacity increases in the order of fixed bed, fluidised bed and entrained bed [56]. Among the three gasifiers, fixed bed gasifier is the most attractive gasifier in terms of low capital investment, simple operation and allowing large variation of feedstock [60]. Updraft and downdraft fixed-bed gasifiers have been widely used in the industry. The main difference between these two gasifiers lies in the direction of feedstock and air supplies into the reactor. In the updraft fixed bed gasifier, the feedstock is fed from the top while the air is fed from the bottom [56]. In the downdraft fixed-bed gasifier, the feedstock is supplied from the top and the air is introduced above the reduction zone [60]. Such different configuration leads to the presence of different reaction zones at different locations in the reactor. The advantage of updraft gasifier lies in the relatively low temperature (200–300 °C) of the gas leaving the gasifier unit, which gives relatively high overall energy efficiency. However, updraft gasifier may generate high tar-containing gas product, which requires additional post-treatment equipment. In contrast, downdraft gasifier generally produces low tar-containing gas product due to the occurrence of partial cracking of the tar in the gas as the gas passes through the high temperature zone in the gasifier [56]. Depending on the desirable tar content in the gas product, either of these gasifiers is recommended for gasification of oil palm biomass.

Fermentation process can also be considered to produce bioethanol from oil palm biomass. In this 2-step process, enzymes are initially used to convert the complex sugar polymer (i.e., hemicellulose and cellulose) into fermentable sugar and yeast is subsequently used to convert fermentable sugar into bioethanol [61]. For this process, OPT and OPF serve as the most suitable feedstock given their highest hemicellulose and cellulose content relative to PKS, MF and EFB [40–42]. The presence of lignin in OPT and OPF, nonetheless, translates to the requirement for an additional pre-treatment process to break down lignin that cannot be decomposed by reactions with enzymes [62].

Conclusion

The thermal decomposition behaviours of OPT, PKS, OPF, MF and EFB were studied under oxidative and non-oxidative conditions using thermogravimetric-mass spectrometry (TG-MS). The strongly overlapped thermal decomposition regions for hemicellulose, cellulose and lignin manifested into complex thermal decomposition for these five oil palm biomass that depends upon the relative amount of these three components in each biomass and/or the catalytic effect from the inorganic constituents. Hemicellulose and cellulose decompositions in the five oil palm biomass were dominated by phase boundary reaction while lignin decomposition in five oil palm biomass and char oxidation in OPT, OPF and EFB were governed by nucleation. Char oxidation in PKS and MF, nonetheless, was jointly controlled by phase boundary reaction and nucleation. MS profiles reveal that the pyrolysis of OPT and OPF leads to significant H_2 and CO_2 emission above 600 °C from self-gasification although negligible weight losses were indicated in TG profiles of OPT and OPF beyond 600 °C. Such self-gasification was not observed in the pyrolysis of PKS, MF and EFB. In combustion of OPT, OPF and PKS, two distinct peaks are depicted on the H_2O evolution profile from 280 to 450 °C and on the CO_2 evolution profile from 450 to 580 °C, which was not found in the H_2O and CO_2 evolution profiles from the combustion of MF and EFB. The catalytic inorganics in the oil palm biomass or their inherent composition could promote such evolution during combustion.

Acknowledgements Jiuan Jing Chew and Jaka Sunarso gratefully acknowledge the Research Micro Fund Internal Grants provided by the Swinburne University of Technology Sarawak Campus ("Characterization of oil palm biomass for thermochemical processing" and "Evaluating the gaseous emission from thermochemical processing of biomass").

Compliance with Ethical Standards

Conflict of Interest The authors declare that they have no competing financial interest.

References

1. MPOC (2012) The oil palm tree. Malaysia Palm Oil Council (MPOC). http://www.mpoc.org.my/The_Oil_Palm_Tree.aspx. Accessed 20/06/2018

2. Agricultural area in Malaysia (2017) Food and Agriculture Organization of the United Nations (FAOSTAT). http://www.fao.org/faostat/en/#country/131. Accessed 07/09/2018
3. Mohammed MAA, Salmiaton A, Wan Azlina WAKG, Mohammad Amran MS, Fakhru'l-Razi A, Taufiq-Yap YH (2011) Hydrogen rich gas from oil palm biomass as a potential source of renewable energy in Malaysia. Renew Sust Energ Rev 15(2):1258–1270. https://doi.org/10.1016/j.rser.2010.10.003
4. Aljuboori A (2013) Oil palm biomass residue in Malaysia: availability and sustainability. Int J Biomass Renew 2:13–18
5. Garcia-Nunez JA, Ramirez-Contreras NE, Rodriguez DT, Silva-Lora E, Frear CS, Stockle C, Garcia-Perez M (2016) Evolution of palm oil mills into bio-refineries: literature review on current and potential uses of residual biomass and effluents. Resour Conserv Recycl 110:99–114. https://doi.org/10.1016/j.resconrec.2016.03.022
6. Palm oil biomass (2013) Sarawak Energy. http://www.sarawakenergy.com.my/index.php/r-d/biomass-energy/palm-oil-biomass. Accessed 09/09/2018
7. Basiron Y, Weng CK (2004) The oil palm and its sustainability. J Oil Palm Res 16(1):1–10
8. Demirbaş A (2001) Biomass resource facilities and biomass conversion processing for fuels and chemicals. Energy Conv Manag 42(11):1357–1378. https://doi.org/10.1016/S0196-8904(00)00137-0
9. McKendry P (2002) Energy production from biomass (part 2): conversion technologies. Bioresour Technol 83(1):47–54. https://doi.org/10.1016/S0960-8524(01)00119-5
10. Chen W-H, Lin B-J, Huang M-Y, Chang J-S (2015) Thermochemical conversion of microalgal biomass into biofuels: a review. Bioresour Technol 184:314–327. https://doi.org/10.1016/j.biortech.2014.11.050
11. Luangkiattikhun P, Tangsathitkulchai C, Tangsathitkulchai M (2008) Non-isothermal thermogravimetric analysis of oil-palm solid wastes. Bioresour Technol 99(5):986–997. https://doi.org/10.1016/j.biortech.2007.03.001
12. Patel M, Zhang X, Kumar A (2016) Techno-economic and life cycle assessment on lignocellulosic biomass thermochemical conversion technologies: a review. Renew Sust Energ Rev 53:1486–1499. https://doi.org/10.1016/j.rser.2015.09.070
13. Awalludin MF, Sulaiman O, Hashim R, Nadhari WNAW (2015) An overview of the oil palm industry in Malaysia and its waste utilization through thermochemical conversion, specifically via liquefaction. Renew Sust Energ Rev 50:1469–1484. https://doi.org/10.1016/j.rser.2015.05.085
14. Yang H, Yan R, Chen H, Zheng C, Lee DH, Liang DT (2006) In-depth investigation of biomass pyrolysis based on three major components: hemicellulose, cellulose and lignin. Energy Fuel 20(1):388–393. https://doi.org/10.1021/ef0580117
15. Jahirul IM, Rasul GM, Chowdhury AA, Ashwath N (2012) Biofuels production through biomass pyrolysis—a technological review. Energies 5(12):4952–5001. https://doi.org/10.3390/en5124952
16. Guo J, Lua AC (2001) Kinetic study on pyrolytic process of oil-palm solid waste using two-step consecutive reaction model. Biomass Bioenergy 20(3):223–233. https://doi.org/10.1016/S0961-9534(00)00080-5
17. Vyazovkin S, Burnham AK, Criado JM, Pérez-Maqueda LA, Popescu C, Sbirrazzuoli N (2011) ICTAC Kinetics Committee recommendations for performing kinetic computations on thermal analysis data. Thermochim Acta 520(1):1–19. https://doi.org/10.1016/j.tca.2011.03.034
18. Šesták J, Berggren G (1971) Study of the kinetics of the mechanism of solid-state reactions at increasing temperatures. Thermochim Acta 3(1):1–12. https://doi.org/10.1016/0040-6031(71)85051-7
19. Šimon P (2011) Fourty years of the Šesták–Berggren equation. Thermochim Acta 520(1):156–157. https://doi.org/10.1016/j.tca.2011.03.030
20. Shen DK, Gu S, Luo KH, Bridgwater AV, Fang MX (2009) Kinetic study on thermal decomposition of woods in oxidative environment. Fuel 88(6):1024–1030. https://doi.org/10.1016/j.fuel.2008.10.034
21. Lee XJ, Lee LY, Gan S, Thangalazhy-Gopakumar S, Ng HK (2017) Biochar potential evaluation of palm oil wastes through slow pyrolysis: thermochemical characterization and pyrolytic kinetic studies. Bioresour Technol 236:155–163. https://doi.org/10.1016/j.biortech.2017.03.105
22. McKendry P (2002) Energy production from biomass (part 1): overview of biomass. Bioresour Technol 83(1):37–46. https://doi.org/10.1016/S0960-8524(01)00118-3
23. Huang YF, Kuan WH, Chiueh PT, Lo SL (2011) Pyrolysis of biomass by thermal analysis–mass spectrometry (TA–MS). Bioresour Technol 102(3):3527–3534. https://doi.org/10.1016/j.biortech.2010.11.049
24. Sanchez-Silva L, López-González D, Villaseñor J, Sánchez P, Valverde JL (2012) Thermogravimetric–mass spectrometric analysis of lignocellulosic and marine biomass pyrolysis. Bioresour Technol 109:163–172. https://doi.org/10.1016/j.biortech.2012.01.001
25. López-González D, Fernandez-Lopez M, Valverde JL, Sanchez-Silva L (2013) Thermogravimetric-mass spectrometric analysis on combustion of lignocellulosic biomass. Bioresour Technol 143:562–574. https://doi.org/10.1016/j.biortech.2013.06.052
26. Asadieraghi M, Daud WMAW (2015) In-depth investigation on thermochemical characteristics of palm oil biomasses as potential biofuel sources. J Anal Appl Pyrolysis 115:379–391. https://doi.org/10.1016/j.jaap.2015.08.017
27. Aghamohammadi N, Nik Sulaiman NM, Aroua MK (2011) Combustion characteristics of biomass in SouthEast Asia. Biomass Bioenergy 35(9):3884–3890. https://doi.org/10.1016/j.biombioe.2011.06.022
28. Bridgwater AV (2012) Review of fast pyrolysis of biomass and product upgrading. Biomass Bioenergy 38:68–94. https://doi.org/10.1016/j.biombioe.2011.01.048
29. Xiong S, Zhuo J, Zhang B, Yao Q (2013) Effect of moisture content on the characterization of products from the pyrolysis of sewage sludge. J Anal Appl Pyrolysis 104:632–639. https://doi.org/10.1016/j.jaap.2013.05.003
30. Tsai WT, Lee MK, Chang YM (2006) Fast pyrolysis of rice straw, sugarcane bagasse and coconut shell in an induction-heating reactor. J Anal Appl Pyrolysis 76(1):230–237. https://doi.org/10.1016/j.jaap.2005.11.007
31. Loh SK (2017) The potential of the Malaysian oil palm biomass as a renewable energy source. Energy Conv Manag 141:285–298. https://doi.org/10.1016/j.enconman.2016.08.081
32. Idris SS, Rahman NA, Ismail K (2012) Combustion characteristics of Malaysian oil palm biomass, sub-bituminous coal and their respective blends via thermogravimetric analysis (TGA). Bioresour Technol 123:581–591. https://doi.org/10.1016/j.biortech.2012.07.065
33. Sami M, Annamalai K, Wooldridge M (2001) Co-firing of coal and biomass fuel blends. Prog Energy Combust Sci 27(2):171–214. https://doi.org/10.1016/S0360-1285(00)00020-4
34. Cheng K, Winter WT, Stipanovic AJ (2012) A modulated-TGA approach to the kinetics of lignocellulosic biomass pyrolysis/combustion. Polym Degrad Stab 97(9):1606–1615. https://doi.org/10.1016/j.polymdegradstab.2012.06.027
35. Stefanidis SD, Kalogiannis KG, Iliopoulou EF, Michailof CM, Pilavachi PA, Lappas AA (2014) A study of lignocellulosic biomass pyrolysis via the pyrolysis of cellulose, hemicellulose and

lignin. J Anal Appl Pyrolysis 105:143–150. https://doi.org/10.1016/j.jaap.2013.10.013
36. Kai X, Yang T, Huang Y, Sun Y, He Y, Li R (2011) The effect of biomass components on the co-combustion characteristics of biomass with coal. In: Second International Conference on Digital Manufacturing & Automation, 2011, pp 1274–1278. https://doi.org/10.1109/ICDMA.2011.314
37. Szabó P, Várhegyi G, Till F, Faix O (1996) Thermogravimetric/mass spectrometric characterization of two energy crops, Arundo donax and Miscanthus sinensis. J Anal Appl Pyrolysis 36(2):179–190. https://doi.org/10.1016/0165-2370(96)00931-X
38. Idris SS, Rahman NA, Ismail K, Alias AB, Rashid ZA, Aris MJ (2010) Investigation on thermochemical behaviour of low rank Malaysian coal, oil palm biomass and their blends during pyrolysis via thermogravimetric analysis (TGA). Bioresour Technol 101(12):4584–4592. https://doi.org/10.1016/j.biortech.2010.01.059
39. Yin CY, Kadir SASA, Lim YP, Syed-Ariffin SN, Zamzuri Z (2008) An investigation into physicochemical characteristics of ash produced from combustion of oil palm biomass waste in a boiler. Fuel Process Technol 89(7):693–696. https://doi.org/10.1016/j.fuproc.2007.12.012
40. Ang SK, Shaza EM, Adibah Y, Suraini AA, Madihah MS (2013) Production of cellulases and xylanase by Aspergillus fumigatus SK1 using untreated oil palm trunk through solid state fermentation. Process Biochem 48(9):1293–1302. https://doi.org/10.1016/j.procbio.2013.06.019
41. Chew J-J, Doshi V, Yong S-T, Bhattacharya S (2016) Kinetic study of torrefaction of oil palm shell, mesocarp and empty fruit bunch. J Therm Anal Calorim 126(2):709–715. https://doi.org/10.1007/s10973-016-5518-3
42. Khalil HPSA, Alwani MS, Ridzuan R, Kamarudin H, Khairul A (2008) Chemical composition, morphological characteristics, and cell wall structure of Malaysian oil palm fibers. Polym Plast Technol Eng 47(3):273–280. https://doi.org/10.1080/03602550701866840
43. Ma Z, Chen D, Gu J, Bao B, Zhang Q (2015) Determination of pyrolysis characteristics and kinetics of palm kernel shell using TGA–FTIR and model-free integral methods. Energy Conv Manag 89:251–259. https://doi.org/10.1016/j.enconman.2014.09.074
44. Lopez-Velazquez MA, Santes V, Balmaseda J, Torres-Garcia E (2013) Pyrolysis of orange waste: a thermo-kinetic study. J Anal Appl Pyrolysis 99:170–177. https://doi.org/10.1016/j.jaap.2012.09.016
45. Collard F-X, Blin J (2014) A review on pyrolysis of biomass constituents: mechanisms and composition of the products obtained from the conversion of cellulose, hemicelluloses and lignin. Renew Sust Energ Rev 38:594–608. https://doi.org/10.1016/j.rser.2014.06.013
46. Özsin G, Pütün AE (2017) Kinetics and evolved gas analysis for pyrolysis of food processing wastes using TGA/MS/FT-IR. Waste Manag 64:315–326. https://doi.org/10.1016/j.wasman.2017.03.020
47. Gunasee SD, Carrier M, Gorgens JF, Mohee R (2016) Pyrolysis and combustion of municipal solid wastes: evaluation of synergistic effects using TGA-MS. J Anal Appl Pyrolysis 121:50–61. https://doi.org/10.1016/j.jaap.2016.07.001
48. Yan J, Jiang X, Han X, Liu J (2013) A TG–FTIR investigation to the catalytic effect of mineral matrix in oil shale on the pyrolysis and combustion of kerogen. Fuel 104:307–317. https://doi.org/10.1016/j.fuel.2012.10.024
49. López-González D, Fernandez-Lopez M, Valverde JL, Sanchez-Silva L (2014) Gasification of lignocellulosic biomass char obtained from pyrolysis: kinetic and evolved gas analyses. Energy 71:456–467. https://doi.org/10.1016/j.energy.2014.04.105
50. Ren Q, Zhao C (2012) NO_x and N_2O precursors from biomass pyrolysis: nitrogen transformation from amino acid. Environ Sci Technol 46(7):4236–4240. https://doi.org/10.1021/es204142e
51. Darvell LI, Jones JM, Gudka B, Baxter XC, Saddawi A, Williams A, Malmgren A (2010) Combustion properties of some power station biomass fuels. Fuel 89(10):2881–2890. https://doi.org/10.1016/j.fuel.2010.03.003
52. Balat M, Balat M, Kırtay E, Balat H (2009) Main routes for the thermo-conversion of biomass into fuels and chemicals. Part 1: pyrolysis systems. Energy Conv Manag 50(12):3147–3157. https://doi.org/10.1016/j.enconman.2009.08.014
53. Sun X, Shan R, Li X, Pan J, Liu X, Deng R, Song J (2017) Characterization of 60 types of Chinese biomass waste and resultant biochars in terms of their candidacy for soil application. GCB Bioenergy 9(9):1423–1435. https://doi.org/10.1111/gcbb.12435
54. Madhiyanon T, Sathitruangsak P, Sungworagarn S, Fukuda S, Tia S (2013) Ash and deposit characteristics from oil-palm empty-fruit-bunch (EFB) firing with kaolin additive in a pilot-scale grate-fired combustor. Fuel Process Technol 115:182–191. https://doi.org/10.1016/j.fuproc.2013.05.018
55. Obernberger I (1998) Decentralized biomass combustion: state of the art and future development. Biomass Bioenergy 14(1):33–56. https://doi.org/10.1016/S0961-9534(97)00034-2
56. McKendry P (2002) Energy production from biomass (part 3): gasification technologies. Bioresour Technol 83(1):55–63. https://doi.org/10.1016/S0960-8524(01)00120-1
57. Nanou P, van Rossum G, van Swaaij WPM, Kersten SRA (2011) Evaluation of catalytic effects in gasification of biomass at intermediate temperature and pressure. Energy Fuel 25(3):1242–1253. https://doi.org/10.1021/ef101557b
58. Nipattummakul N, Ahmed II, Kerdsuwan S, Gupta AK (2012) Steam gasification of oil palm trunk waste for clean syngas production. Appl Energy 92:778–782. https://doi.org/10.1016/j.apenergy.2011.08.026
59. Atnaw SM, Sulaiman SA, Yusup S (2013) Syngas production from downdraft gasification of oil palm fronds. Energy 61:491–501. https://doi.org/10.1016/j.energy.2013.09.039
60. Guangul FM, Sulaiman SA, Ramli A (2012) Gasifier selection, design and gasification of oil palm fronds with preheated and unheated gasifying air. Bioresour Technol 126:224–232. https://doi.org/10.1016/j.biortech.2012.09.018
61. Sarkar N, Ghosh SK, Bannerjee S, Aikat K (2012) Bioethanol production from agricultural wastes: an overview. Renew Energy 37(1):19–27. https://doi.org/10.1016/j.renene.2011.06.045
62. Noparat P, Prasertsan P, O-Thong S, Pan X (2017) Sulfite pretreatment to overcome recalcitrance of lignocellulose for enzymatic hydrolysis of oil palm trunk. Energy Procedia 138:1122–1127. https://doi.org/10.1016/j.egypro.2017.10.209